JOURNAL OF GEOPHYSICAL RESEARCH, VOL. 113, B08310, doi:10.1029/2007JB005410, 2008

Improved tests reveal that the accelerating moment release hypothesis is statistically insignificant

Jeanne L. Hardebeck,[1] Karen R. Felzer,[2] and Andrew J. Michael[1]

Received 27 September 2007; revised 21 March 2008; accepted 7 April 2008; published 12 August 2008.

[1] We test the hypothesis that accelerating moment release (AMR) is a precursor to large earthquakes, using data from California, Nevada, and Sumatra. Spurious cases of AMR can arise from data fitting because the time period, area, and sometimes magnitude range analyzed before each main shock are often optimized to produce the strongest AMR signal. Optimizing the search criteria can identify apparent AMR even if no robust signal exists. For both 1950–2006 California-Nevada $M \geq 6.5$ earthquakes and the 2004 M9.3 Sumatra earthquake, we can find two contradictory patterns in the pre–main shock earthquakes by data fitting: AMR and decelerating moment release. We compare the apparent AMR found in the real data to the apparent AMR found in four types of synthetic catalogs with no inherent AMR. When spatiotemporal clustering is included in the simulations, similar AMR signals are found by data fitting in both the real and synthetic data sets even though the synthetic data sets contain no real AMR. These tests demonstrate that apparent AMR may arise from a combination of data fitting and normal foreshock and aftershock activity. In principle, data-fitting artifacts could be avoided if the free parameters were determined from scaling relationships between the duration and spatial extent of the AMR pattern and the magnitude of the earthquake that follows it. However, we demonstrate that previously proposed scaling relationships are unstable, statistical artifacts caused by the use of a minimum magnitude for the earthquake catalog that scales with the main shock magnitude. Some recent AMR studies have used spatial regions based on hypothetical stress loading patterns, rather than circles, to select the data. We show that previous tests were biased and that unbiased tests do not find this change to the method to be an improvement. The use of declustered catalogs has also been proposed to eliminate the effect of clustering but we demonstrate that this does not increase the statistical significance of AMR. Given the ease with which data fitting can find desired patterns in seismicity, future studies of AMR-like observations must include complete tests against synthetic catalogs that include spatiotemporal clustering.

Citation: Hardebeck, J. L., K. R. Felzer, and A. J. Michael (2008), Improved tests reveal that the accelerating moment release hypothesis is statistically insignificant, *J. Geophys. Res.*, *113*, B08310, doi:10.1029/2007JB005410.

1. Introduction

[2] This study examines whether or not accelerating moment release (AMR) [e.g., *Bowman et al.*, 1998; see also *Mignan et al.*, 2006a, and references therein] is a statistically significant precursor to large earthquakes in California and Nevada. While a number of studies of the AMR hypothesis have reported positive results, our study is motivated by concerns that the existence of a number of free parameters in this hypothesis could lead to false positive results if the effects of data fitting are not considered carefully. In particular, *Bowman et al.* [1998] adjust the region and time that they inspect before each main shock to optimize AMR, although theoretically, if a gradual elastic build up of strain is the true cause of the acceleration, as claimed by *Bowman et al.* [1998], the AMR signal should not be very sensitive to the space and time window.

[3] Searching seismicity catalogs for precursors to large earthquakes has been an active avenue of research for many years. This course of research is reasonable because the obvious temporal and spatial clustering of earthquakes demonstrates that events interact with each other. This line of inquiry is also appealing because earthquake catalogs cover the entire globe, and, although their quality varies as both a function of space and time, these catalogs are generally easy to obtain. However, it should be noted that seismicity represents only part of the deformation processes involved in plate tectonics and seismogenesis and thus provides only a limited view into possible precursory

[1] U.S. Geological Survey, Menlo Park, California, USA.
[2] U.S. Geological Survey, Pasadena, California, USA.

behavior. Proposed seismicity precursors range from simple changes in the rate of seismicity such as quiescence and activation, to those that include spatial patterns such as Mogi-doughnuts [for overviews, see *Kanamori*, 1981; *Reyners*, 1981], to complex systems such as M8 [*Keilis-Borok and Kossobokov*, 1990] and Pattern Informatics [*Tiampo et al.*, 2006].

[4] AMR is a more sophisticated version of the activation hypothesis based on the concept that earthquakes are an example of a critical point phenomena. According to the activation hypothesis one expects a precursory increase in the rate of earthquakes before a large event. In the AMR hypothesis as formalized by *Bowman et al.* [1998], the rate of seismicity increases such that the cumulative Benioff strain (square root of the seismic moment or energy) [*Benioff*, 1951] follows a power-law function until the time of an eventual main shock. Thus it falls under the broad category of seismicity rate changes. *Reasenberg and Matthews* [1988] looked for rate changes before 32 $M \geq 5.3$ earthquakes in central California (from 1974 to 1986) and Japan (from 1926 to 1984). If the statistics of each of the 32 sequences they studied are considered separately, then they found statistically significant (at the 90% confidence level) activation before 4 of the sequences, statistically significant quiescence before 3 of the sequences, and no significant rate changes before the remaining 25 sequences. Thus, if each sequence were considered as an individual case study, 7 of them could contribute to the literature on either activation or quiescence. However, taken as an ensemble the result is clearly that there is no consistent, precursory pattern of seismicity rate changes before earthquakes. The lesson of *Matthews and Reasenberg* [1988] is clear: case studies are not sufficient and we must test such hypotheses by looking at an entire catalog of data.

[5] Given the results of *Matthews and Reasenberg* [1988], it is reasonable to ask why one should continue to study the possibility that there are precursory rate changes before large earthquakes. There are two differences between AMR and the method used by Matthews and Reasenberg. First, AMR quantifies the seismicity by the cumulative Benioff strain while Matthews and Reasenberg used the number of earthquakes over a given magnitude. This difference is important if the magnitude-frequency relationship has temporal variations so that the count of earthquakes over a given magnitude is not proportional to the Benioff strain. Temporal variations in the magnitude-frequency relationship are certainly possible and some have argued that there are precursory variations in the *b-value* from the Gutenberg-Richter relationship [*Reyners*, 1981]. The second difference is that AMR hypothesizes a gradual change in the seismicity while Matthews and Reasenberg used a method optimized for sudden changes in the rate. While the method of Matthews and Reasenberg should detect clear examples of AMR, it is possible that it could miss some borderline cases. Thus it is reasonable to do a study specifically of the AMR hypothesis.

[6] Our study will focus on the AMR hypothesis as presented by *Bowman et al.* [1998]. This frequently cited paper is an important underpinning to current research because it clearly formalized the AMR concept into a testable hypothesis and introduced tests to estimate the statistical significance of the results. These tests used synthetic seismicity catalogs to determine how often AMR could be observed by random chance. Thus the paper of *Bowman et al.* [1998] was an important step forward. Our study is motivated by concerns that their tests may have underestimated the importance of data fitting by treating each main shock in isolation (rather than considering a complete catalog of events) and lacked sufficient statistical power because too few sequences were analyzed. Also, *Bowman et al.* [1998] tested their results using synthetic catalogs that did not include spatiotemporal clustering.

[7] To test the AMR hypothesis, we first investigate the effects of data fitting by searching for both AMR and decelerating moment release (DMR) in both the California-Nevada catalog and before the 2004 M9.3 Sumatra-Andaman Islands earthquake. Second, we compare the frequency of AMR before large earthquakes in the actual California-Nevada earthquake catalog with results obtained using synthetic seismicity catalogs that contain no AMR. Multiple methods will be used to synthesize these catalogs to ensure that the results are robust and not dependent on details of how the synthetic catalog is produced. Third, we test the stability of scaling relationships between the duration and spatial extent of apparent AMR patterns and the magnitude of the earthquakes that follow.

[8] Our tests are more rigorous than the tests done by *Bowman et al.* [1998] and other AMR literature in several ways. Most importantly, we analyze the real data and synthetics identically, which has not been done in any prior study of AMR of which we are aware. The data and synthetics must be treated exactly the same, so that any differences in the observed AMR behavior are clearly differences in the catalogs rather than differences in the analysis. In order to make sure that the analysis is done uniformly, we use clearly defined search parameters and avoid ad hoc decisions when determining the amount of AMR in the data and synthetics. We also compare AMR in the real catalogs with AMR in synthetic catalogs containing spatial-temporal clustering and multiple main shocks. Synthetics used in prior work have considered only one main shock, and have not included earthquake clustering. Because our synthetics contain spatial-temporal clustering, they more closely resemble real seismicity than the uniform random seismicity considered by *Bowman et al.* [1998] and other prior studies.

[9] In the years since the paper of *Bowman et al.* [1998] was published, various authors have proposed changes to the AMR method. Thus, if we focus only on the paper of *Bowman et al.* [1998], our conclusions could be outdated. For instance, *Bowman et al.* [1998] searched for AMR within circular regions around the large earthquakes. *Bowman and King* [2001] introduced search regions based on the Coulomb stress transfer pattern from a backslip model of the main shock, based on the hypothesis that AMR would occur in the regions that are being loaded by the deformation that loads the main shock fault plane. The utility of this hypothesis was tested using California seismicity by *Mignan et al.* [2006a] and we will further examine this hypothesis. *Mignan et al.* [2006a] also used declustered earthquake catalogs to try to reduce the effect of clustering and we will test whether or not this affects the statistical significance of the results. By doing

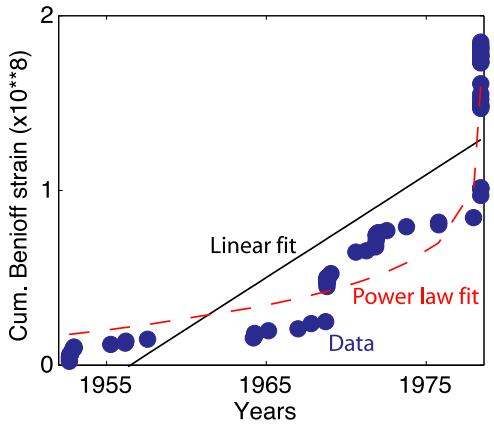

Figure 1. Example of fitting a power-law (red dashed line) and linear function (black line) to the data (blue circles). For this example, which is from an ETAS simulation of an earthquake catalog, $C = 0.4$.

so we ensure that our conclusions are applicable to the current state of the art.

2. Methods of Measuring AMR and Statistical Significance

[10] *Bowman et al.* [1998] formalized the search for AMR by developing a measure of whether the cumulative Benioff strain before an earthquake is better fit by a power-law function or a linear function with respect to time (Figure 1). The cumulative Benioff strain, $\varepsilon(t)$, is determined for a given radius around, and during a time period before, a main shock:

$$\varepsilon(t) = \sum_{i=1}^{N(t)} E_i(t)^{1/2} \tag{1}$$

where E_i is the energy of the ith event at time t and $N(t)$ is the number of events up to time t. We assume that $\log_{10}(E)$ is proportional to 1.5 times the magnitude [e.g., *Kanamori and Anderson*, 1975] but our results do not depend on the specific empirical relationship.

[11] Two temporal functions are then fit to the cumulative Benioff strain curve: a linear function and a power-law function. The power-law function is:

$$\varepsilon(t) = A + B(t_c - t)^m \tag{2}$$

where t_C is the time of the main shock, B is negative, and $0 < m < 1$ for the power-law to be concave upward. To fit equation (2) to equation (1), the parameter A is set to the cumulative Benioff strain at the time of, and including, the main shock.

[12] Finally, to produce a measure of the degree of AMR before a main shock, *Bowman et al.* [1998] introduced the parameter C:

$$C = \frac{\text{power law fit root} - \text{mean} - \text{square error}}{\text{linear fit root} - \text{mean} - \text{square error}} \tag{3}$$

If the power-law fits the observed cumulative Benioff strain better than the linear function, C will be less than 1. *Bowman et al.* [1998] require $m \leq 0.8$ so that the power-law function will not approximate a linear function. If the power-law function does not fit the data as well as the linear function, C will be greater than 1.

[13] The C value depends on the earthquakes used to determine $\varepsilon(t)$ and the earthquakes used depend on the size of the region selected around the main shock, the time period before the main shock, the magnitude range used to select the data, and the minimum number of earthquakes required to define a pattern. The magnitude range used by *Bowman et al.* [1998] is 2 units smaller than the main shock except when they concluded that the catalog was complete to a lower level. Because such ad hoc decisions cannot be automated we will use the magnitude range of 2 units smaller than the main shock. The region around the main shock is determined by adjusting the radius of the region until the minimum C value is obtained, although *Bowman et al.* [1998] do not use a uniform search criteria. *Bowman et al.* [1998] do not discuss how the time period used before each main shock is chosen, but since the amount of time used before each main shock varies, presumably these time periods have also been optimized to maximize AMR. We want to essentially follow the protocol of *Bowman et al.* [1998] but wish to make the optimization procedure more uniform so that our results are readily reproducible. We find that we get very similar results to those of *Bowman et al.* [1998] if we use an optimization method of varying the radius of the region around the main shock from 20 km to 1000 km in steps of 20 km, and varying the start time before the main shock from the beginning of the catalog to the year before the main shock in steps of 1 year.

[14] Another issue is whether C varies with the minimum number of earthquakes required for calculating an AMR solution ($N_{\min}$). *Bowman et al.* [1998] note that acceleration cannot be measured with fewer than 4 earthquakes and set $N_{\min} = 4$. *Mignan et al.* [2006a] use $N_{\min} = 5$. Bowman (personal communication) has suggested, however, that spuriously low C values might be calculated when data sets of earthquakes are very small and has suggested $N_{\min} = 10$. We measure how C varies in the real catalog when we use $N_{\min}$ values of 4, 6, 8, and 10. We observe a small increase in mean C when $N_{\min}$ is increased from 4 to 8. The values for $N_{\min} = 8$ and $N_{\min} = 10$ are the same, but with a larger sample we might observe a difference. Thus, to be conservative, we do all of our comparisons between the synthetics and real data using both $N_{\min} = 4$, in accordance with *Bowman et al.* [1998], and $N_{\min} = 10$, in accordance with Bowman's later advice.

[15] *Bowman et al.* [1998] define a successful AMR detection if $C \leq 0.7$, while other studies [e.g., *Mignan et al.*, 2006b] use different threshold values of C. When we do our tests we look at the full distribution of C values for a catalog of main shocks, so that we are sensitive to the full range of apparent AMR behavior.

[16] We present the distributions of C values for the real and synthetic data as cumulative density functions (CDFs). If the real catalog exhibits more distinct accelerations than the synthetic catalogs, the distribution for the real data should be larger for smaller values of C than the distribution for the synthetics. Then, in the plots, the CDF curve for the real data should lie above and to the left of the CDF curve for the synthetics. To visually estimate the uncertainty in

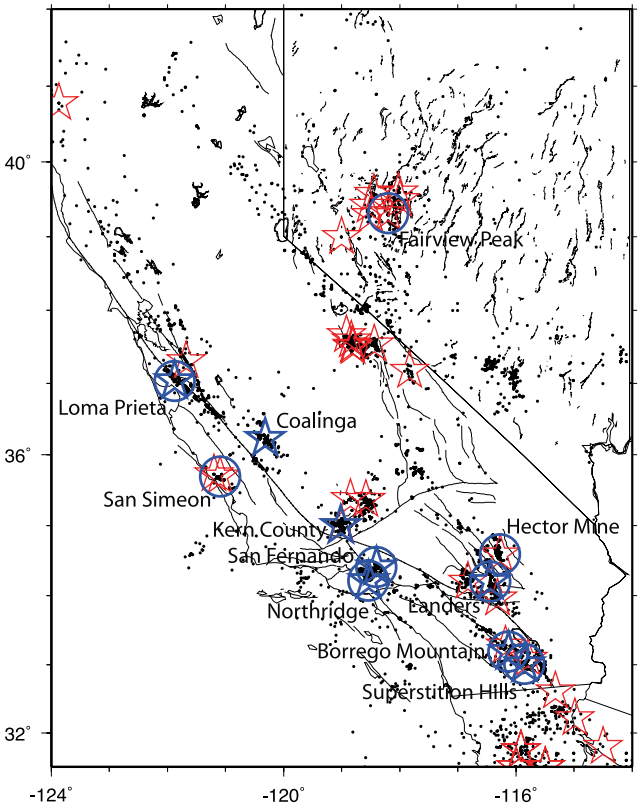

Figure 2. Map showing the region analyzed with earthquakes M $\geq$ 4 as black dots, earthquakes M $\geq$ 6 as red stars, main shocks analyzed by *Bowman et al.* [1998] as blue stars, main shocks included in our test of searching for AMR based on prestress patterns as blue circles, and faults and state borders as lines.

these CDFs, we also plot the 95% confidence regions of the cumulative density functions as determined by bootstrap resampling of the distributions. The bootstrap resampling assumes that the individual C values are independent, although in reality they are not because the data-selection regions for multiple main shocks can overlap. Thus the bootstrap resampling slightly underestimates the true variability in the CDFs and thus this visual representation may make the distributions of the real and synthetic data look more distinct than they actually are.

[17] Finally, we use a Kolmogorov-Smirnov (K-S) test to test the null hypothesis that the distribution of C for the real main shocks is not biased toward lower values of C than the distribution of C for the synthetic main shocks. Because the distribution of C for the synthetic main shocks is an observation with uncertainty, this K-S test is done as a two-sample test. Because we test whether the real distribution is biased in one direction from the synthetic distribution it is a one-tailed test. We present the results of this test as the confidence that we can reject the null hypothesis. When this confidence is over 95% we accept that more AMR is present in the real data than in the synthetic catalogs. Note that the K-S test also assumes that the individual C values are independent and thus also slightly overestimates the statistical significance of AMR in the real data. Therefore our tests are conservative with respect to falsely rejecting the AMR hypothesis and could accept it even when it should be rejected.

3. Data

[18] When we search for AMR before real earthquakes we use the ANSS catalog for California and Nevada, available from the Northern California Earthquake Data Center (www.ncedc.org/anss, last accessed on March 27, 2006) for the time period from 1950 to 2005. We define the California and Nevada region as from 31.5° to 42°N and 114° to 124°W (Figure 2).

[19] *Bowman et al.* [1998] studied the 8 M $\geq$ 6.5 earthquakes occurring after 1950 in California as well as the 1986 M_L 5.6 Palm Springs earthquake and 3 smaller and larger global earthquakes. This is a very small data set with which to do statistical tests since, as we will show later, it is so easy to find apparent AMR signals in random data sets. *Bowman et al.* [1998] only used main shocks in California, although Nevada was part of their study region and they included Nevada seismicity in their searches for AMR. No reason is given for the lack of Nevada main shocks, so we add in main shocks located in Nevada. A number of papers have claimed to observe AMR worldwide, and the smaller Nevada earthquakes are already included in the analysis so there are no additional concerns about catalog coverage or completeness, so including Nevada main shocks should not influence our results. This increases our sample size to 15 M $\geq$ 6.5 main shocks, but this is still a very small sample.

[20] One important question is how large an earthquake has to be to qualify as a "main shock". We can increase the sample size by including smaller earthquakes as main shocks, but only if we can demonstrate that the degree of acceleration before our new main shocks matches what is seen before the M $\geq$ 6.5 events. When *Bowman et al.* [1998] analyze smaller events they caution that for smaller main shocks the seismic acceleration might be obscured by stress redistribution from larger earthquakes. We evaluate whether it is possible to drop our main shock magnitude to M 6 by calculating C values before 42 M $\geq$ 6 California/Nevada earthquakes. After eliminating two main shocks with C values that are >1, one of which was M>6.5, we measure the linear correlation coefficient between main shock magnitude and C. We find no significant correlation (the linear correlation coefficient, r^2, is 0.02 for the 40 earthquakes), indicating that lowering the main shock magnitude to M 6 does not change the AMR behavior of the sample. Using even smaller main shocks could improve our statistics further but would require us to use earthquakes smaller than M 4 to search for the AMR, which would dip below the magnitude completeness threshold of the 1950–2005 catalog.

[21] The final step in our data selection is that we limit our entire earthquake catalog to be post-1950. *Bowman et al.* [1998] also use primarily post-1950 data, but for the 1952 Kern County and 1989 Loma Prieta earthquakes they go back to 1910 to search for acceleration. *Bowman et al.* [1998] do note that this can be problematic, as one expects to see apparent seismicity rate accelerations from 1910 to 1949 because of improved detection of earthquakes. Routine and consistent magnitude determination began in

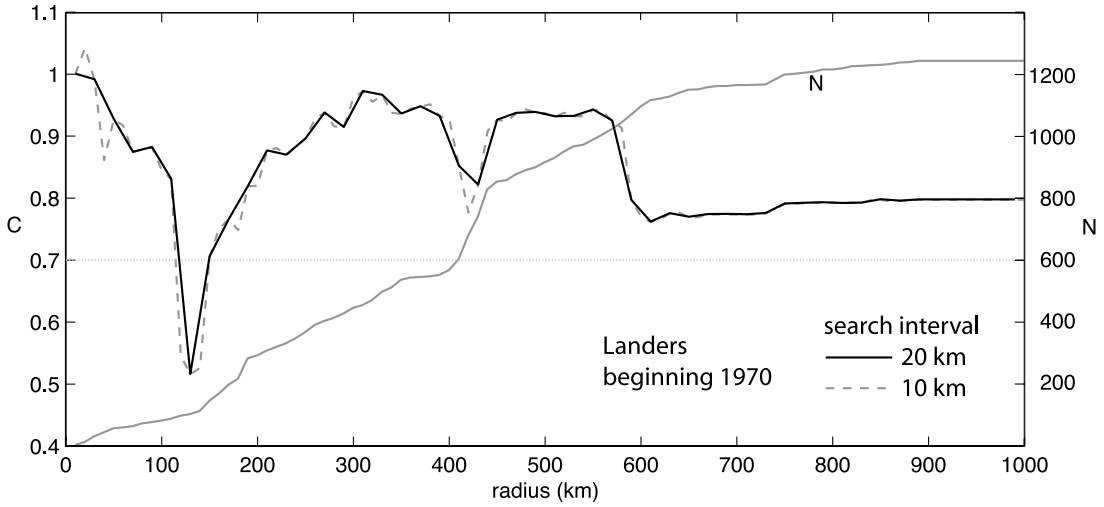

Figure 3. *C* versus radius, for the 1992 Landers earthquake, with both 10 and 20 km search steps, using all events M $\geq$ 4. The beginning of the time interval is fixed to 1970, which produces the lowest *C* value over all start times and radii. The total number of events, *N*, is also shown.

Southern California in 1932 and in Northern California in 1948 [*Uhrhammer et al.*, 1996]. *Bowman et al.* [1998] attempt to correct for this by using only M $\geq$ 5.5 earthquakes from this period, but the statewide completeness magnitude was actually > M 6 [*Toppozada and Branum*, 2002], or as large as the main shocks themselves, and magnitude errors were high. Further significant improvements to the seismic network in the 1970s and late 1990s may also create artificial acceleration in the catalog, but to a lesser extent since in many areas of the state the improvement affected detection of earthquakes smaller than the M $\geq$ 4 shocks that we use here.

[22] We find that starting the catalog in 1950 rather than 1910 does not bias our results against the AMR hypothesis. AMR can be found before the Loma Prieta earthquake without going back to 1950. For the 1952 Kern County earthquake it is true that a low *C* value cannot be found using only post-1950 data. If true acceleration was occurring before this earthquake it seems odd that it should not be apparent in the two years immediately preceding the main shock. Nonetheless, we find that we can simply remove the Kern County earthquake from the database without affecting our statistical results.

[23] We also note that extending the catalog back in time for some, but not all earthquakes, is a form of special pleading (changing the rules for specific cases with no set guidelines) and this makes it difficult to do a proper statistical test because one would have to consider the special pleading for each of the main shocks in the synthetic data sets. The one exception we make is for our DMR tests (see below), for which we do go back to 1910 for the Kern County earthquake. However, the DMR tests are done to demonstrate the power of data fitting and we do not make statistical tests of these results.

4. Decelerating Moment Release and the Power of Data Fitting

[24] The value of *C* is highly sensitive to the search radius (Figure 3). Increasing the radius adds spatial clusters of earthquakes that may contribute to or counteract AMR, and *C* changes accordingly. *C* is also sensitive to the catalog starting time. Temporal clusters of events near the end of the catalog contribute to AMR, while those near the beginning counteract it. Because *C* is unstable with respect to search radius, we hypothesize that low *C* may be found in data sets with no true AMR, and therefore apparent AMR may be the result of data fitting.

[25] The power of data fitting to find any desired seismicity pattern can be demonstrated by searching for a different pattern, for example a deceleration of seismicity rate, prior to the same main shocks that are cited as being preceded by AMR. If significant decelerating moment release (DMR) is found before many of the main shocks cited as examples of AMR, then the most plausible explanation is that both patterns are the result of data fitting.

[26] Searches for DMR require just two changes to the use of equation (2). First the restriction $m \geq 1$ is applied to produce curves that are concave downward. Second, *A* is left a free parameter because fixing it to the cumulative Benioff strain, including that of the main shock, would destroy any apparent deceleration. We then use the same parameter *C* to measure the strength of the DMR.

[27] To find DMR we first study the eight M $\geq$ 6.5 California main shocks for which *Bowman et al.* [1998] reported AMR, and we use the same earthquake catalog to search for these seismicity trends. DMR is found before all 8 main shocks, and in each case the DMR is significant according to *Bowman et al.*'s [1998] criteria of $C < 0.7$ (Figure 4). The optimal radii and time windows are similar to those for AMR, so AMR and DMR are not characteristic of different length or time scales (Table 1).

[28] We next search for both AMR and DMR before all M $\geq$ 6 main shocks that occurred after 1950 in the ANSS catalog for California and Nevada. Figure 5 shows the cumulative distribution of the observed curvature parameter *C* for the optimal AMR and DMR before each main shock. Although the *C* value distributions for AMR and DMR are not directly comparable statistically because of the difference

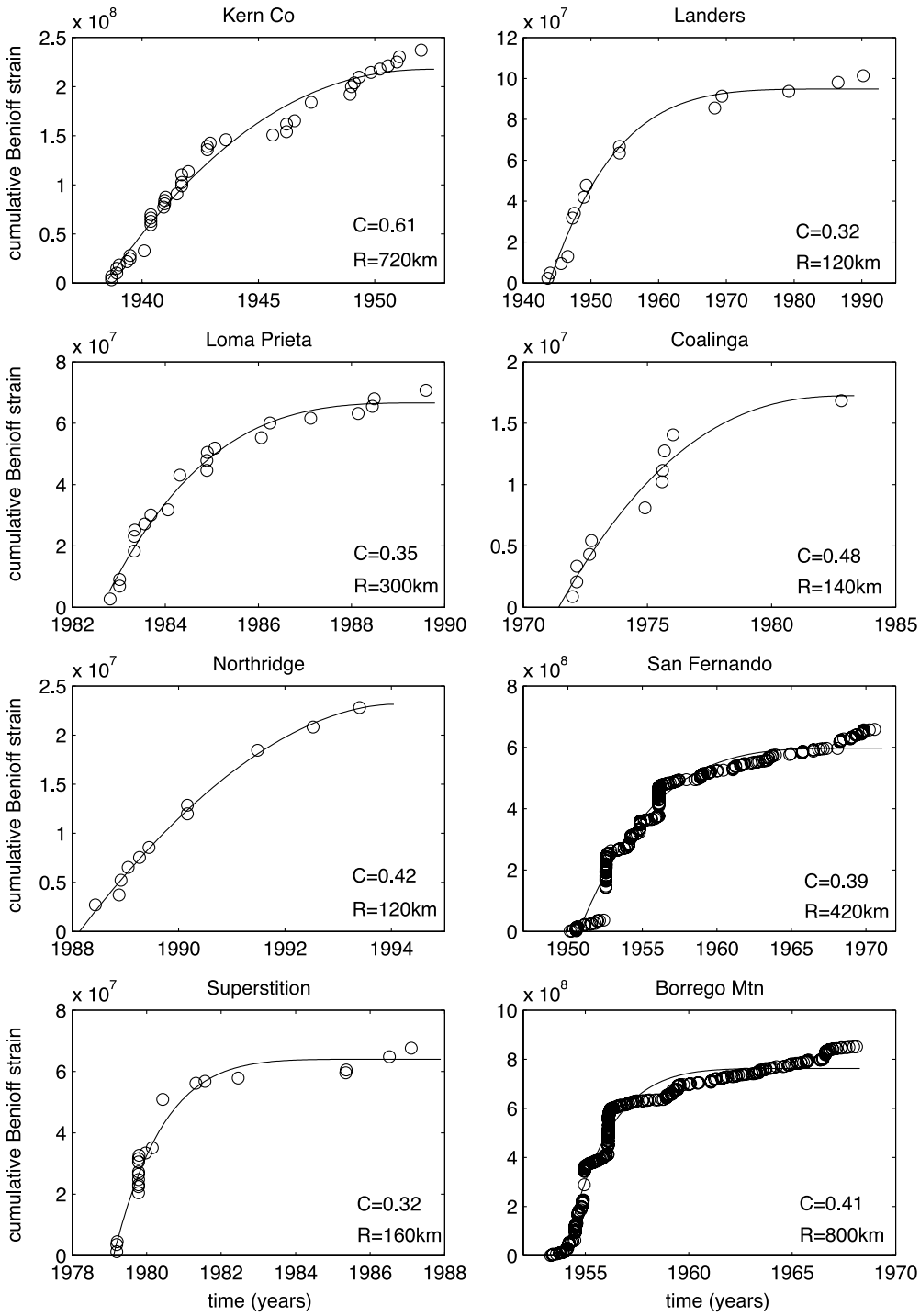

Figure 4. Optimal decelerating moment release (DMR) curves for the 8 California M $\geq$ 6.5 main shocks for which *Bowman et al.* [1998] report AMR. *C* is the curvature parameter, and R is the optimal radius.

in whether A is fixed or treated as a free parameter, it is clear that there are nearly as many main shocks with well-resolved DMR signals (low *C*) as with well-resolved AMR signals. Many main shocks exhibit both AMR and DMR for different data-selection choices.

[29] Another example of data fitting is for the December 2004 M9.3 Sumatra earthquake. Two studies [*Jiang and Wu*, 2005; *Mignan et al.*, 2006b] report significant AMR prior to this event beginning around 1980. Following *Mignan et al.* [2006b], we use shallow events (depth $\leq$40 km) from the ANSS global earthquake catalog from 1965 to 2004 (www.ncedc.org/anss, last accessed on February 16, 2007). We consider a catalog containing all events M $\geq$ 4.5, and, because the M $\geq$ 4.5 catalog is clearly not complete [see *Mignan et al.*, 2006b, Figure A1], we also consider a catalog containing all M $\geq$ 5.5 events. While *Mignan et al.* [2006b]

Table 1. Optimal Length Scale and Time Scale for AMR [from *Bowman et al.*, 1998] and DMR (This Study) for 8 California Main Shocks

Earthquake, d/mo/yr	AMR Length Scale, km [*Bowman et al.*, 1998]	AMR Length Scale, km [This Study]	DMR Length Scale, km	AMR Time Scale, yr [*Bowman et al.*, 1998]	AMR Time Scale, yr [This Study]	DMR Time Scale, yr
Kern County, 21 Jul 1952	325	360	720	42	42	14
Landers, 28 Jun 1992	150	40	120	22	44	49
Loma Prieta, 18 Oct 1989	200	60	300	79	79	7
Coalinga, 2 May 1983	175	180	140	3	4	12
Northridge, 17 Jan 1994	73	380	120	2	38	6
San Fernando, 9 Feb 1971	100	140	420	4	9	21
Superstition Hills, 24 Nov 1987	275	100	160	6	7	9
Borrego Mtn., 9 Apr 1968	240	280	800	10	9	15

search for AMR in regions based on Coulomb stress modeling, we search for AMR and DMR using circular regions. We show in section 6.3 that the difference in region shape does not make a significant difference in the identification of AMR for California and Nevada.

[30] Both significant AMR and significant DMR ($C < 0.7$) are found in the pre–Sumatra earthquake catalogs (Figure 6). The optimal AMR curve for the M $\geq$ 4.5 catalog (Figure 6a) is similar to the curve of *Mignan et al.* [2006b], verifying that the difference in region shape is not greatly important. The C value for the M $\geq$ 4.5 DMR curve is somewhat higher than for the M $\geq$ 4.5 AMR curve, which is probably the result of the incompleteness of the M $\geq$ 4.5 catalog. An incomplete catalog will become more complete through time, producing an artifact of apparently increasing seismicity rate. For the more complete M $\geq$ 5.5 catalog, the C values for the optimal AMR and DMR curves are more similar. The optimal AMR curves begin around 1980, while the optimal DMR curves begin around 2000. Much of the data fitting in the Sumatra case depends on two M7.9 events occurring in June 2000 (one in Sumatra, one in the Indian Ocean). If these events occur near the end of the selected time window, apparent AMR is observed, while if these events occur near the beginning, apparent DMR is observed. Note that the AMR and DMR curves contain a similarly large number of events, so no argument can be made that the AMR curve is more real on the basis of the large number of events that define it.

[31] There is no significance to the longer time scale of apparent AMR than DMR for the Sumatra example. For the eight California events studied by *Bowman et al.* [1998], the optimal time scales and length scale for DMR overlap with those for AMR (Table 1). One example of an earthquake with a longer time scale of apparent DMR is the 1971 San Fernando earthquake. Optimal DMR is found starting in 1950 (Figure 4 and Table 1) while optimal AMR starts in 1967 [see *Bowman et al.*, 1998, Figure 6]. In this case, the data fitting involves a period of low seismicity rate during 1956–1968. If the selected window begins during this time, apparent AMR is observed, while if this time occurs later in the time window, apparent DMR is observed. This example and the Sumatra example demonstrate how fluctuations in the background seismicity rate can be selected to produce the desired seismicity pattern.

[32] None of these examples should be taken to imply that DMR is a real precursory process. Instead, these examples demonstrate that two contrary signals, accelerating and decelerating seismicity, can often be found in the same data set. It seems implausible that true acceleration and deceleration are simultaneously present, strongly suggesting that both signals are found as a result of data fitting.

5. Synthetic Seismicity Tests

[33] We further consider the possibility that AMR is not a real physical process, and that it is found before many main shocks because the time and area windows are adjusted to optimize for acceleration. If this explanation is correct, AMR should be found at a similar rate in real catalogs and in synthetic catalogs in which no real AMR is present. We perform this test by generating suites of synthetic catalogs and searching them for AMR in the same way as the real catalogs. The null hypothesis is that the synthetic catalogs contain as much AMR as the real catalog. A rejection of this null hypothesis would support AMR as a real physical phenomenon. If the null hypothesis cannot be rejected, this would support our theory that AMR is an artifact of data fitting. As discussed in section 2, we use the

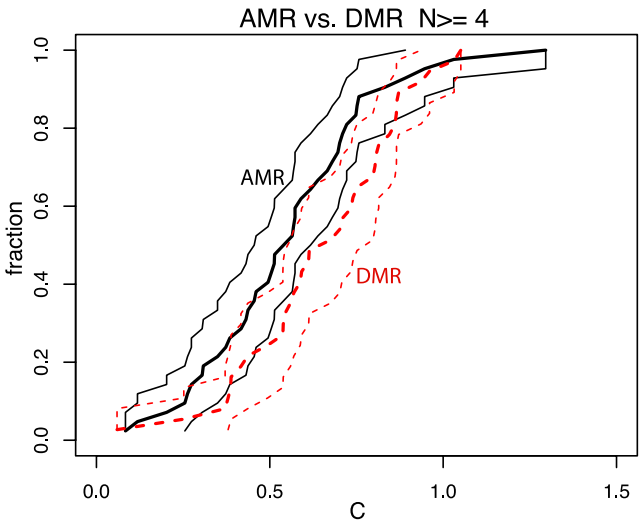

Figure 5. Cumulative distribution of the observed curvature parameter C for the optimal AMR (black lines) and DMR (red dashed lines) before each M $\geq$ 6 main shock in the ANSS catalog for California and Nevada, since 1950. The thick lines show the best result and the thin lines show the 95% confidence region determined by bootstrap resampling.

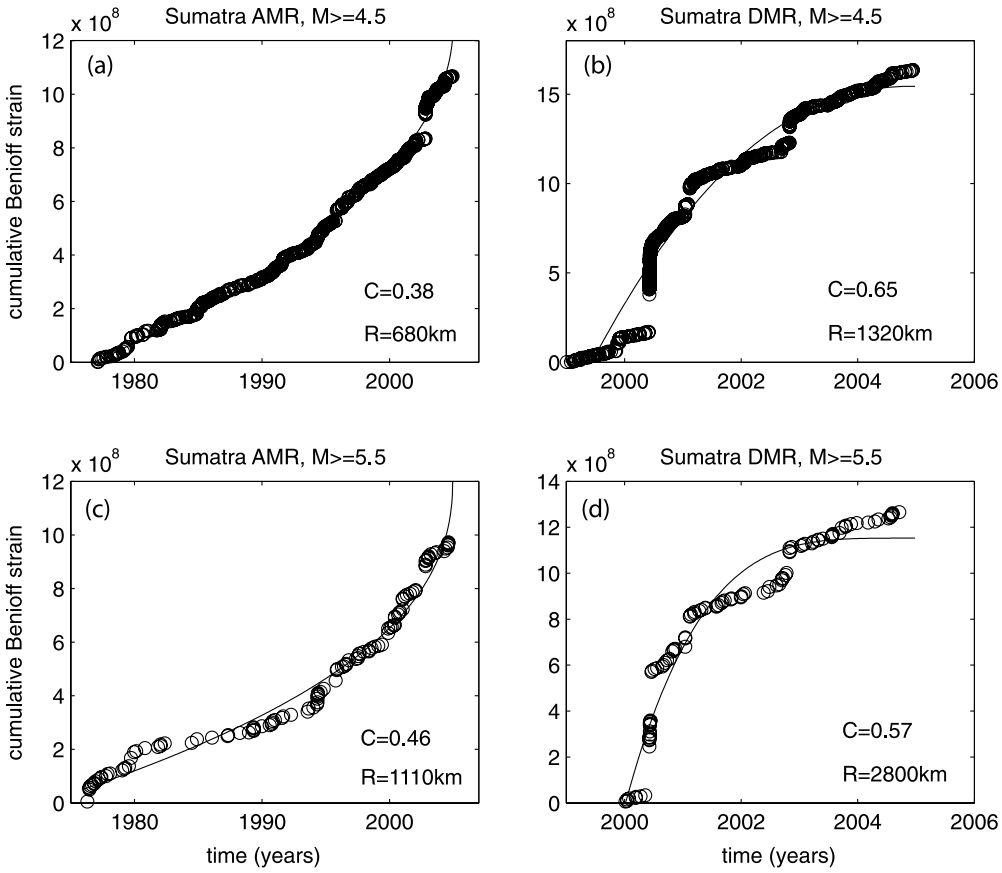

Figure 6. Optimal AMR and DMR for the December 2004 M9.1 Sumatra earthquake, using minimum magnitudes of 4.5 and 5.5. *C* is the curvature parameter, and R is the optimal radius. Note that the data are not complete to magnitude 4.5; but that level is included for comparison with the study of *Mignan et al.* [2006b].

95% confidence level as the test of whether or not the null hypothesis can be rejected.

5.1. Synthetic Seismicity Catalogs

[34] We generate four types of synthetic test catalogs using different approaches. These catalogs range from purely random earthquake times and locations to more complex catalogs based on two epidemic-type aftershock sequence (ETAS) models [e.g., *Ogata*, 1988] that include both spatiotemporal earthquake clustering and a spatial distribution of background seismicity based on the real data. Each synthetic catalog is designed to contain approximately the same number of events as the real catalog, and to span the same spatial area and duration.

5.1.1. Uniform Random Seismicity Catalogs

[35] The first type of synthetic catalog is the simplest, consisting of uniform random seismicity. The number of events in each synthetic catalog matches the number in the real ANSS CA-NV catalog. The synthetic event locations and times are randomly selected from a uniform distribution over the spatial and temporal range of the real ANSS catalog. The magnitudes are selected randomly, without replacement, from the distributions of magnitudes in the real catalog. We generate 10 simulated catalogs in this way, for a grand total of 420 main shocks. This method produces synthetic seismicity that matches the number of earthquakes and the magnitude distribution from the real catalog but does not produce realistic spatial or temporal clustering behavior (Figures 7c and 7d).

5.1.2. Random Times/Real Locations Catalogs

[36] The next type of synthetic catalog more resembles real seismicity in that it contains the same spatial clustering as the real data. The real earthquake locations are used, while the synthetic earthquake times and magnitudes are assigned randomly as before. Again we generate 10 simulated catalogs in this way, containing a total of 420 main shocks. This method produces synthetic seismicity that matches the number of earthquakes, magnitude distribution, and spatial pattern of the real catalog but does not include realistic temporal clustering (Figures 7e and 7f).

5.1.3. ETAS Synthetic Seismicity Catalogs

[37] The third and fourth sets of synthetic catalogs consist of ETAS simulations [e.g., *Ogata*, 1988] that include spatiotemporal earthquake clustering (Figures 7g–7j). The times of the background earthquakes are chosen randomly, using a spatially varying (on a 0.5° grid) background seismicity rate found from the real ANSS catalog using the technique of *Hainzl et al.* [2006]. For the magnitude distribution for the third set of simulations we assign the magnitude of each earthquake randomly from the Gutenberg-Richter distribution with a *b* value of 1.0, following *Felzer et al.* [2002]. For the fourth set of simulations we

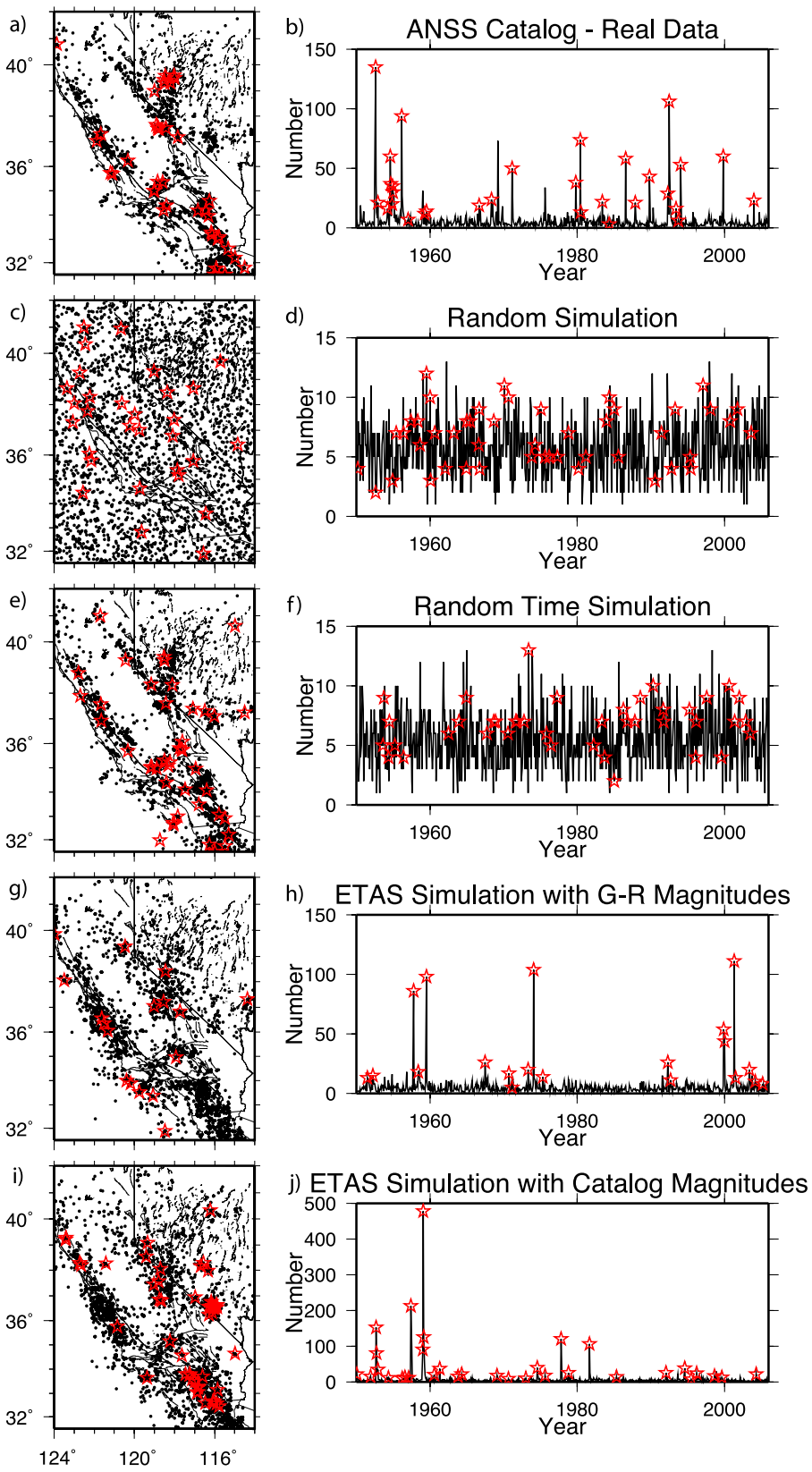

Figure 7. Maps and time series of the real data from the ANSS catalog and examples of the four simulation methods used in the paper. The maps show earthquakes M $\geq$ 4 as black dots, earthquakes M $\geq$ 6 as red stars, and faults and state borders as lines. The time series show the number of earthquakes per month with the occurrence of earthquakes M $\geq$ 6 as red stars.

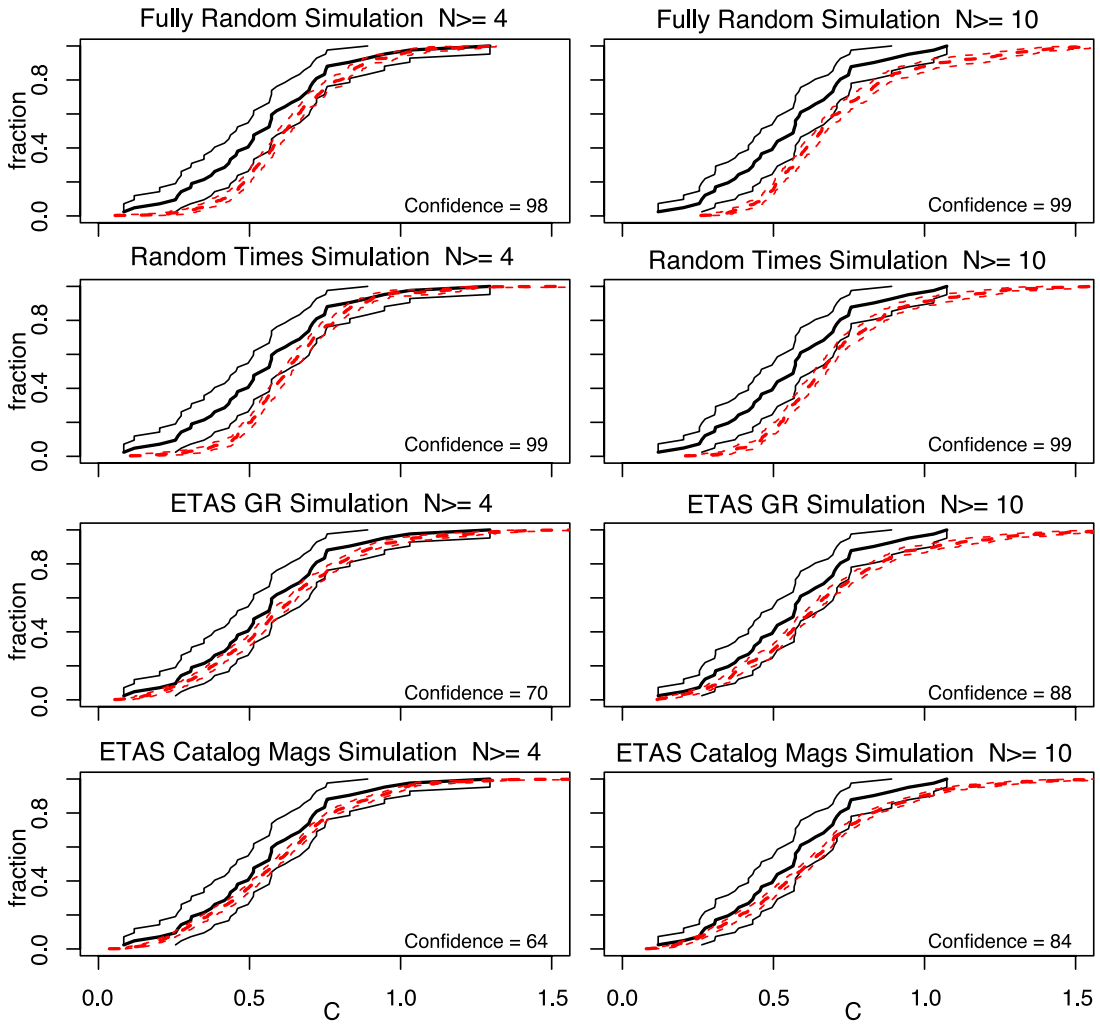

Figure 8. Cumulative distribution of the observed curvature parameter C for the optimal AMR determined from the real ANSS catalog (black lines) and each of the four simulation methods (red dashed lines) before each M $\geq$ 6 main shock. Results for both $N_{min} = 4$ and $N_{min} = 10$ are shown. The thick lines show the best result and the thin lines show the 95% confidence region determined by bootstrap resampling. The confidence is the level at which we can reject the null hypothesis that the C values for the real data are not lower than the C values for the synthetic data, e.g., the confidence of accepting AMR.

choose magnitudes randomly from the magnitudes listed in the ANSS catalog. Note that the total number of earthquakes in each ETAS simulation and in the ANSS catalog will not necessarily be the same, and thus some magnitudes will be randomly omitted or repeated.

[38] Our synthetic ETAS catalogs do not exactly match the number of earthquakes in the original catalogs, or the sharpness of the fault system, but do produce spatial and temporal clustering resembling real data. For the purposes of this study, we believe that these catalogs are adequate. Further details on the ETAS simulations are presented in the Appendix A.

5.2. Synthetic Seismicity Results

[39] The cumulative density functions (CDF) of the C values for the real data and the synthetic catalogs are shown in Figure 8. The CDF curves, with the 95% confidence regions estimated using a bootstrap approach, provide a visual comparison between the results from the real data and the synthetic catalogs while the statistical significance estimated using a K-S test provides an objective measure of whether or not the null hypothesis (that the real catalog does not produce more AMR than the simulated catalogs) can be rejected.

[40] It is clear that increasing N_{min} has only a small effect on the results. Higher N_{min} does increase the statistical significance of AMR but in no case does the difference between $N_{min} = 4$ and $N_{min} = 10$ change whether or not the null hypothesis can be rejected. For most main shocks, the number of events in the optimal sequence, N, is greater than N_{min} (Figure 9a). Low values of C arise in sequences with a range of values of N, and hence are not an artifact of small data sets (Figure 9a).

[41] However, whether or not we reject the null hypothesis is dependent on whether or not the synthetic catalogs contain spatiotemporal earthquake clustering. The CDFs for the two types of synthetic catalogs without spatiotemporal

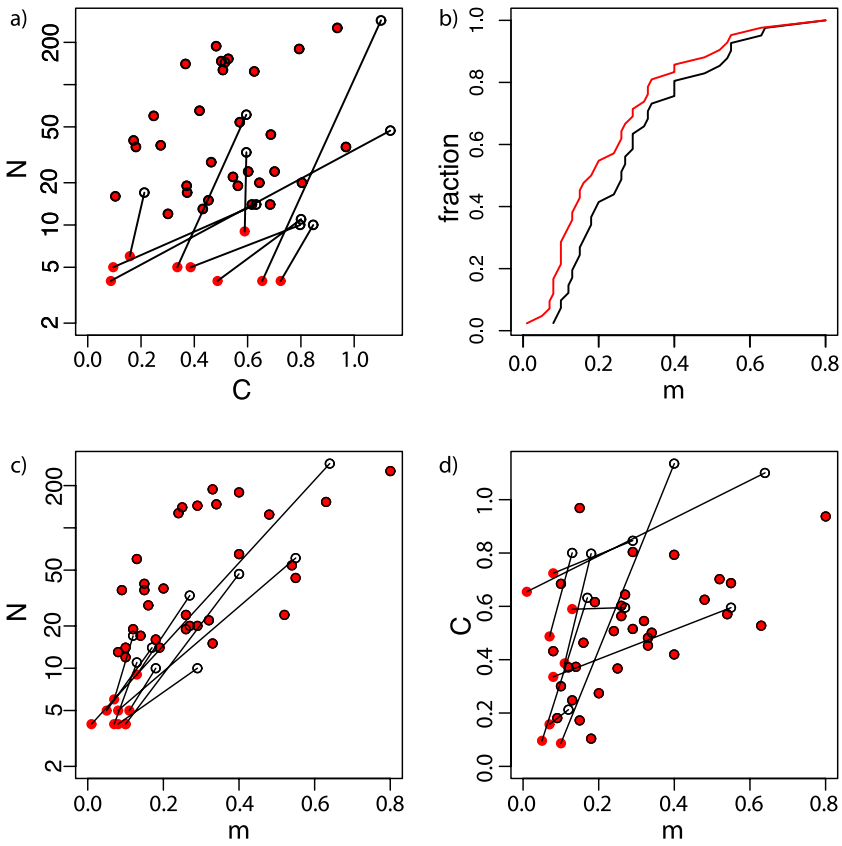

Figure 9. Parameters for optimal AMR for the real California-Nevada catalog, for N_{min} = 4 (red) and N_{min} = 10 (black). (a) Number of events in the optimal sequence, N, versus C. Lines connect points for the same main shock for different N_{min}. (b) Cumulative distribution of the power-law exponent m. (c) N versus m. (d) C versus m.

clustering, the uniform random seismicity and the randomized earthquake catalog, show significantly less AMR than the CDF for the real data at above 95% confidence. For the two ETAS simulations, which contain spatiotemporal clustering, we cannot reject at 95% confidence the null hypothesis that the CDFs for the synthetics contain as much AMR as the CDF for the real data.

[42] The cumulative distribution curves for the real and ETAS catalogs exhibit a steep slope starting at $C \approx 0$, indicating that both data sets include main shocks preceded by distinct and well-resolved accelerations with small C. The CDFs for the synthetic data sets without spatiotemporal clustering have a shallow slope for very small values of C and become steep only for larger values of C, indicating that few of the non-ETAS synthetic main shocks are associated with AMR with very small (less than ~0.2) C values.

[43] The rate and strength of AMR observed in real and ETAS seismicity catalogs is the same, despite the fact that no real AMR exists in the ETAS catalogs. The spatiotemporal seismicity clustering contributes to the apparent AMR, because each earthquake may become a foreshock by directly or indirectly triggering a main shock. When the rate of seismicity is higher than usual, the probability of a main shock being triggered is also higher and this may look like AMR. We conclude that AMR is observed before many main shocks both because of the clustering process and because a search is done for the spatial and temporal extent of the region that optimizes the AMR signal.

6. Scaling Relationships

[44] The size of the region over which AMR is observed has been reported to scale with the magnitude of the eventual main shock [e.g., *Bowman et al.*, 1998]. This apparent scaling is often used as an argument in support of AMR as the result of a real physical process, since a critical region of increased loading would reasonably scale with the size of the eventual rupture. The time period over which AMR is observed also appears to scale with main shock magnitude in their results.

[45] We first investigate the robustness of the proposed scaling relationship between main shock magnitude and the size of the region exhibiting AMR. *Bowman et al.* [1998] proposed a linear scaling relation between the log of the optimal region size and main shock magnitude based on 8 M $\geq$ 6.5 California main shocks, and 4 additional earthquakes that extend the magnitude range. For only 2 of the 8 California events, however, does the confidence region for the optimal radius intersect the scaling relationship curve (their Figure 7). We test for AMR for the same 8 California main shocks, using the radius scaling relation given by *Bowman et al.* [1998] and a duration scaling relationship found from a linear fit of the log of the optimal duration

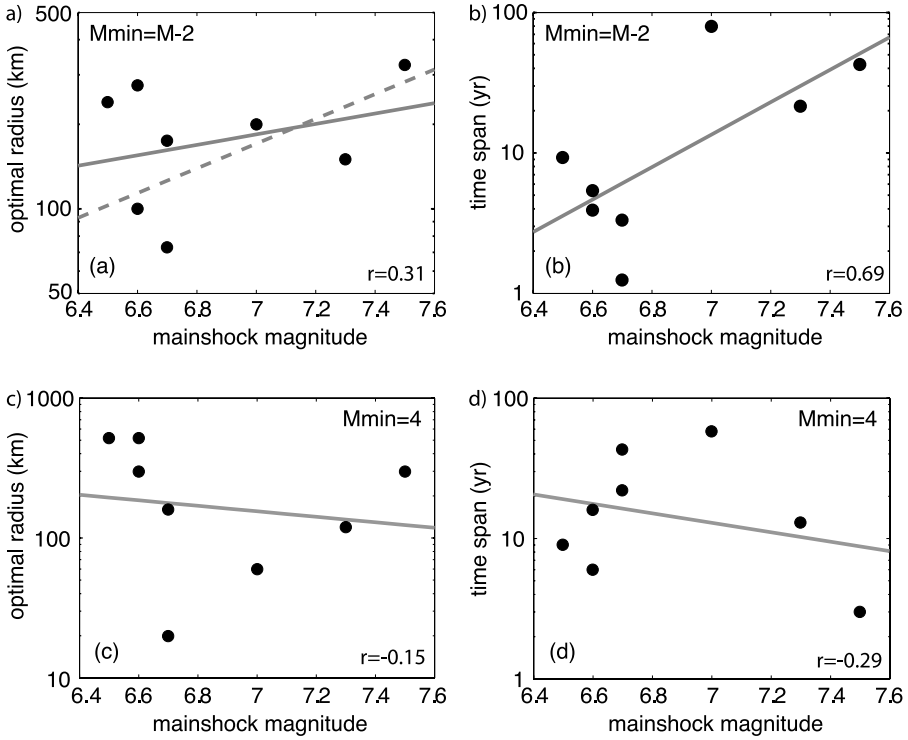

Figure 10. Optimal AMR radius and duration versus main shock magnitude, for eight M $\geq$ 6.5 California earthquakes. Scaling relations were found by least-squares fit of log-radius or log-duration versus magnitude. Correlation coefficient (r) and significance of correlation are also shown. (a) Optimal radii from *Bowman et al.* [1998], found using catalogs with minimum magnitude 2 units below main shock magnitude. Solid line, fit to the 8 California earthquakes; dashed line, *Bowman et al.*'s [1998] fit including 4 additional main shocks to extend the magnitude range. (b) Optimal AMR durations from *Bowman et al.* [1998] (c and d) The optimal radius and duration for each main shock, found using catalogs with fixed minimum magnitude of M4.0. Optimization was performed by grid search to minimize the misfit parameter *C*.

reported by *Bowman et al.* [1998] versus event magnitude (Figure 10b). Using catalogs with spatial and temporal windows defined by these scaling relations, we find no significant AMR ($C < 0.7$) for the 8 California main shocks.

[46] These results imply that the proposed scaling cannot be strictly applied, and in particular cannot be used predictively to estimate the spatial or temporal region in which AMR is expected to occur prior to a given main shock or anticipated future earthquake. The scaling relation is not robust because apparent AMR is very sensitive to the radius and duration of the catalog. The value of *C* can change dramatically over a small increase in region size (Figure 3), as additional earthquake clusters are captured in the region, changing the shape of the cumulative Benioff strain curve. Thus, while the optimal radii and durations found by *Bowman et al.* [1998] roughly scale with magnitude, the difference between the optimal values and the best fit curve translates to a significant difference in *C* value. Therefore the scaling relationships cannot be used to predict the data-selection parameters and avoid the problems of data fitting.

[47] The apparent general increase in optimal region size (Figure 10a) and duration (Figure 10b) could still be used as an argument for a physical basis for AMR, even though particular proposed scaling relationships do not strictly hold. We test whether this apparent scaling is an artifact of data selection. *Bowman et al.* [1998] search for AMR before each main shock using a catalog with a minimum magnitude cutoff two magnitude units below the main shock magnitude. Using a minimum magnitude that scales with the main shock magnitude can affect the apparent optimal region size and AMR duration. For a larger main shock, because of the relative infrequency of larger events, there will be a lower spatial and temporal density of events within two magnitude units, and hence a larger area and/or a longer time period may be needed to accumulate enough events to observe significant AMR. An apparent scaling of optimal region and duration with magnitude could follow.

[48] We examine the dependence of the apparent scaling on minimum magnitude using the same 8 California main shocks studied by *Bowman et al.* [1998]. First we find scaling relationships using the optimal radii and durations reported by *Bowman et al.* [1998]. Because we do not include their additional 4 earthquakes (which would introduce more data-selection issues concerning how these 4 events were chosen), we obtain a somewhat different scaling relationship for radius versus magnitude, but still with a positive slope (Figure 10a). We also find a positive slope for the optimal duration versus magnitude (Figure 10b). For these 8 events, optimal region size and duration weakly scale with main shock magnitude, when the optimization is

performed on catalogs with a minimum magnitude that scales with main shock magnitude.

[49] Next we find the optimal radii and durations for the 8 main shocks using catalogs with a fixed minimum magnitude of M 4.0. In this case, we find no positive correlation of optimal region size or duration with main shock magnitude. The fits to optimal radius versus magnitude (Figure 10c) and optimal duration versus magnitude (Figure 10d) are both essentially flat, with very small negative slopes. Similar results are obtained for minimum magnitudes ranging from M3.0 (probably below the magnitude of completeness) to M4.5 (within 2 magnitude units of the smallest main shocks). There is no scaling of optimal region size or duration with main shock magnitude when the optimization is performed on catalogs with a fixed minimum magnitude. Therefore the apparent radius and duration scaling in this data set is an artifact of using a minimum magnitude that scales with main shock magnitude, and should not be interpreted in terms of physical processes.

7. Tests of Recent Changes in AMR Detection Efforts

[50] In the years since the paper of *Bowman et al.* [1998] was published, several authors have proposed methodological changes to make the search for AMR more effective.

7.1. Coulomb Prestress Regions

[51] One important change is that while *Bowman et al.* [1998] searched for AMR within circular regions around the large earthquakes, *Bowman and King* [2001] used search regions based on the Coulomb stress transfer pattern from a backslip model of the main shock, based on the hypothesis that AMR would occur in the regions that are being loaded by the deformation that loads the main shock fault plane. This method was also advocated by *King and Bowman* [2003] and *Mignan et al.* [2006a, 2006b].

[52] The conceptual model is that the eventual main shock fault patch remains locked, while the rest of the fault slips aseismically at depth and in earthquakes on either side of the locked patch. This is equivalent to modeling back slip on the main shock plane [e.g., *Savage and Burford*, 1973]. Only events in areas of positive Coulomb stress change (ΔCS) in the build up to the main shock are considered when searching for AMR, down to a minimum stress value ΔCSmin, which is chosen to optimize AMR. We test whether using a region based on this hypothetical model of stress loading improves the performance of the AMR model.

[53] We model prestress for nine M $\geq$ 6.5 main shocks in the CA-NV ANSS catalog, using simple main shock slip models with uniform slip on a single fault plane, following *Bowman and King* [2001]. We use published slip models for the San Fernando [*Heaton and Helmberger*, 1979], Superstition Hills [*Wald et al.*, 1990], Loma Prieta [*Wald et al.*, 1991], Landers [*Wald and Heaton*, 1994], Northridge [*Wald et al.*, 1996], Hector Mine [*Ji et al.*, 2002], and San Simeon [*Ji et al.*, 2004] earthquakes. We simplified the models by creating a single fault plane of average strike and dip, and assigning uniform slip to this plane to match the main shock moment. To model the backslip we model slip in the opposite direction from the main shock slip model. For the Fairview Peak main shock, we use the surface rupture from *Caskey et al.* [1996] to determine the location, strike, and length of the rupture, and the moment tensor of *Doser* [1986] to constrain the moment, the fault dip and the rake. For the Borrego Mountain earthquake we use the surface rupture reported by *Allen et al.* [1968] and the moment tensor of *Ebel and Helmberger* [1982]. Because our tests require a minimum of 10 earthquakes before the main shock in both the full and positive prestress regions (N_{min} = 10), we do not use the Kern County, Rainbow Mountain, Stillwater, and Dixie Valley earthquakes, all of which occurred early in the catalog.

[54] We compute the static stress change tensor due to each main shock backslip dislocation, assuming an elastic half-space, using the computer program DLC (R. W. Simpson, personal communication, 2006) based on the subroutines of *Okada* [1992]. We find ΔCS on optimally oriented planes at the hypocenter of each earthquake in the ANSS catalog occurring prior to the main shock. The optimally oriented planes are found assuming that the maximum compressive stress axis of the background stress field is at 45° to the fault plane and that the differential stress is 10 bars, following similar assumptions made by *Bowman and King* [2001]. We also assume an effective coefficient of friction μ = 0.4.

[55] For each of the nine M $\geq$ 6.5 main shocks of the CA-NV ANSS catalog modeled above, we first search for AMR and find the lowest value of C using only events inside the positive prestress region with ΔCS $\geq$ ΔCSmin. As a control, we then separately determine the lowest value of C using earthquakes in both the positive and negative prestress zones by selecting all events with $|\Delta CS| \geq \Delta CSmin$. We find the value of ΔCSmin that optimizes the AMR by stepping through 100 different stress values for ΔCSmin between 0.0001 bars and the largest positive stress change modeled for the earthquake. As in our other tests we find the optimal beginning time by stepping in 1-year increments. If AMR is a real physical process that occurs primarily in the positive prestress zone, then the earthquakes in the positive stress zones should produce a significantly lower C value than the combined shadowed and positive stressed earthquakes. On the other hand, if AMR is unrelated to prestress, for instance if AMR is an artifact of data fitting, the two C values will be comparable.

[56] We find that using the positive prestress region does not significantly improve the performance of the AMR model. Limiting the data set to events with positive prestress produced a lower value of C for only three of the main shocks (Table 2). For 5 of the main shocks, using all of the earthquakes produced a better result, and there was one tie. Limiting the search for AMR to the positive prestress areas therefore does not significantly improve the chances of finding AMR.

7.2. Fixed Curvature Parameter

[57] The approach of *Mignan et al.* [2006a] also differs from our work and the work of *Bowman et al.* [1998] in two important aspects. First, while we follow *Bowman et al.* [1998] and consider the exponent m in equation (2) as a free parameter allowed to range between 0 and 0.8, *Mignan et al.* [2006a] fixed it to m = 0.3 based on the study of *Bufe and Varnes* [1993]. Constraining the exponent m reduces

Table 2. Minimum Value of C for Earthquakes in the Positive Prestress Regions, Compared to Minimum C for All Events[a]

Main Shock, d/mo/yr	C, Positive Prestress Events	C, All Events
Fairview Peak, 16 Dec 1954	**0.28**	0.43
Loma Prieta, 18 Oct 1989	**0.35**	0.43
Hector Mine, 16 Oct 1999	**0.61**	0.68
San Fernando, 9 Feb 1971	**0.52**	**0.52**
San Simeon, 22 Dec 2003	0.7	**0.6**
Borrego Mtn, 9 Apr 1968	1.0	**0.53**
Landers, 28 Jun 1992	0.42	**0.32**
Northridge, 17 Jan 1994	0.85	**0.27**
Superstition Hills, 24 Nov 1987	0.24	**0.05**

[a]Lowest C value for each main shock in bold.

the power of data fitting when fitting the power-law to the data and very low C values will only be found when the data exhibit power-law type behavior with $m \approx 0.3$. This is equally true for the real data and the synthetic catalogs, thus this modification would improve the statistical significance of the AMR hypothesis if the m-exponents in the real data are actually about 0.3.

[58] If the true value of $m \approx 0.3$, we would expect to see the values of m that optimize AMR for the real data to cluster around 0.3. However, we do not find that m tends to be about 0.3 in the real data, but rather that it spans the range of values (Figure 9b). It could be argued that a larger catalog could more precisely determine m, but we find a wide range of optimal m even for data sets with large N (Figure 9c). It is also interesting that the lowest C values correspond to very low m (Figure 9d). This may be an artifact of the definition of C, because when m is very low the power-law is the most different from a line.

[59] When we constrain m to 0.3 and reanalyze the real data and the ETAS simulations, very low C values become more rare in both the real data and the synthetics. Setting m = 0.3 does not improve the statistical significance of the AMR hypothesis (Figure 11). For both $N_{min} = 4$ and $N_{min} = 10$, the null hypothesis, that the synthetic data contains as much AMR as the real data, cannot be rejected with 95% confidence. Because our results show that the m-values found in the real data do not cluster near 0.3 and constraining m to 0.3 does not improve the statistical significance of the AMR signal, our analysis of a larger data set than that of *Bufe and Varnes* [1993] rejects their hypothesis that m is about 0.3.

7.3. Declustering

[60] Second, *Mignan et al.* [2006a] declustered their earthquake catalogs (removed aftershocks) before testing for AMR. The theory behind this change was that aftershocks are not necessarily part of the AMR acceleration and so may detract from detection of the underlying AMR

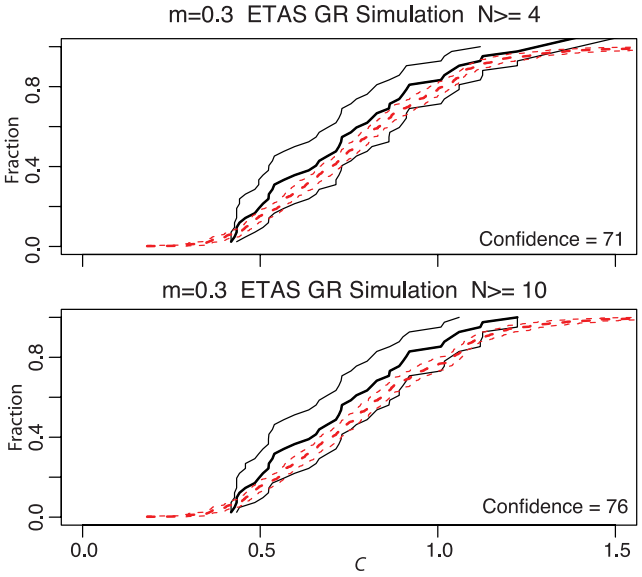

Figure 11. Cumulative distribution of the observed curvature parameter C for optimal AMR, fixing m = 0.3. Distributions are shown for the real ANSS catalog (black lines) and the ETAS simulation methods with G-R magnitudes (red dashed lines) before each M $\geq$ 6 main shock. Results for both $N_{min} = 4$ and $N_{min} = 10$ are shown. The thick lines show the best result and the thin lines show the 95% confidence region determined by bootstrap resampling. The confidence is the level at which we can reject the null hypothesis that the C values for the real data are not lower than the C values for the synthetic data, e.g., the confidence of accepting AMR.

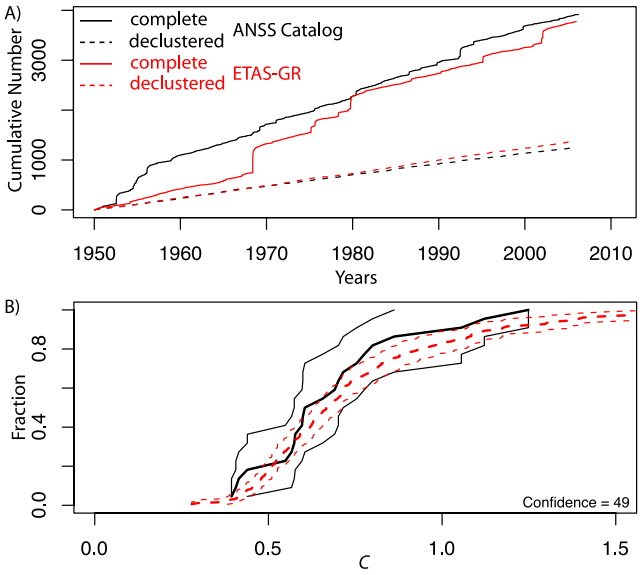

Figure 12. (A) Cumulative number of earthquakes with M $\geq$ 4.0 in the ANSS catalog and an ETAS simulation using a Gutenberg-Richter distribution for the magnitudes. Solid lines show the complete catalogs while the dashed lines show the result of declustering. (B) Cumulative distribution of the observed curvature parameter C for the optimal AMR determined from the real declustered ANSS catalog (black lines) and the declustered ETAS simulations (red dashed lines) before each M $\geq$ 6 main shock. Results for $N_{min} = 10$ are shown. The thick lines show the best result and the thin lines show the 95% confidence region determined by bootstrap resampling. The confidence is the level at which we can reject the null hypothesis that the C values for the real data are not lower than the C values for the synthetic data, e.g., the confidence of accepting AMR.

signal. To test whether declustering improves the performance of the AMR model we used the well known algorithm of *Gardner and Knopoff* [1974] to decluster both the real ANSS catalog and ten synthetic ETAS catalogs, where the synthetic catalogs were produced with magnitudes taken from the Gutenberg-Richter distribution. We then performed new optimizations for AMR, solving for a new C value for each main shock that survived the declustering process. As could be expected from our earlier analysis, declustering caused the overall incidence of low C values to decrease. Furthermore the amount of decrease was similar in the CDFs for the real and synthetic declustered catalogs, such that a K-S test using the CDFs based on the declustered data cannot reject the null hypothesis that the C values of the synthetic data are as low as the C values of the real data (Figure 12). Therefore we find no evidence of the existence of real AMR being concealed by aftershock sequences.

8. Discussion

[61] Determining free parameters from data is often a necessary part of hypothesis development. Given the hypothesis that seismicity accelerates before large earthquakes, it may be reasonable to determine the region and time period over which the acceleration takes place from the data. In AMR studies this is done when the size of the region and length of the time period are determined by minimizing the C value for each earthquake. This practice, frequently referred to as data fitting, carries the danger of identifying patterns that are not real, but are created by choosing the free parameters so that the selected data demonstrates the hypothesized pattern. This danger is particularly high when the results are unstable with respect to small variations in the free parameters. Given that the C value is an unstable function of the selection radius (Figure 3) and time period, the dangers of data fitting with respect to AMR must be carefully considered. This instability also implies that the apparent AMR signals are not the result of a broad regional process but are created by optimally selecting a series of spatial clusters that create an apparent acceleration. The dangers of data fitting are also illustrated by the fact that contrary patterns of accelerating and decelerating moment release can be found in the same, real, data sets by choosing selected radii or time periods.

[62] One way to escape the dangers of data fitting would be to determine these free parameters by some other means. *Bowman et al.* [1998] proposed empirical scaling relationships between the magnitude of the impending main shock and the size of the search region. However, we have demonstrated that this empirical relationship cannot be used to avoid data fitting because when it is used to determine the data-selection area there is no AMR signal. Furthermore, we have demonstrated that this proposed scaling relationship is due to the practice of using a minimum magnitude that scales with the main shock magnitude. Thus the proposed scaling relationships are a statistical artifact of the design of the algorithm and are not evidence of a physical process.

[63] Given the danger that spurious patterns may result from data fitting, it is critical that we test the statistical significance of AMR. We carry out these statistical tests by creating simulated seismicity catalogs, subjecting these simulated catalogs to exactly the same analysis as was applied to the real data, and then determining the probability that the distributions of C values for the real data are lower than the C values for the synthetic catalogs. In this study, we carry out this process using four types of seismicity simulations that each serve to illustrate the important elements of these tests.

[64] The first two seismicity simulations are very simplistic and do not include temporal clustering. The first simulation method creates seismicity that has a random, uniform distribution in time and space and magnitudes are drawn from the real catalog with the rate set to match the rate of earthquakes in the real data. The second simulation differs only in that it uses the locations from the real catalog and thus preserves the spatial characteristics of real data. While many cases of AMR are found in these random catalogs, more are found in the real data and the K-S test rejects the null hypothesis that the synthetic catalogs contain as much AMR as the real catalog. Thus using these simple random catalogs would lead to accepting AMR as a real process. Our second two seismicity simulations do include temporal clustering, however, in the form of aftershocks modeled with an ETAS simulator. When this clustering is included the amount of AMR in the real catalog is not statistically significantly greater than the amount of AMR in the synthetic catalogs.

[65] Important lessons can be drawn from a comparison between the results of our tests using seismicity simulations with the tests done by *Mignan et al.* [2006a]. Their simulations produce distributions of C values where low C values are rare compared to both the real data and to our ETAS simulations. This is because their simulation methods are most similar to our uniform random synthetic seismicity catalogs, which have events uniformly distributed in space and time. However, there are also important differences between their methods and our simple synthetic tests. For instance, our synthetics more realistically represent a full seismicity catalog that includes multiple main shocks, while their catalogs consider individual main shocks in isolation. In their simulations, a cluster of seismicity may only contribute to an AMR signal preceding one earthquake. In our synthetic catalogs, as in real data, a cluster of seismicity exhibiting a rate increase may contribute to the apparent AMR of multiple main shocks, making apparent AMR more common. *Mignan et al.* [2006a] attempt to compensate for the lack of clustering in their simulations by declustering their data. However, declustering algorithms are imperfect and so are unlikely to produce a truly uniform catalog in both space and time. Also, the number of earthquakes in their simulations is set to an artificial number in a nondimensional space rather than being based on the number of earthquakes in the actual catalog with the same spatial size and temporal duration as the real data. Thus the approach of *Mignan et al.* [2006a] does not generate a realistic simulation of the actual data analysis process and this is one of the deficiencies that leads them to underestimate the rate at which low C values will be found by random chance.

[66] *Bowman et al.* [1998] also test the AMR they find against AMR in synthetic catalogs but like *Mignan et al.* [2006a] their synthetics have no spatiotemporal clustering and contain only one synthetic main shock per catalog. Most critically, however, *Bowman et al.* [1998] also eval-

uate their synthetics differently than the real data; whereas the time windows are apparently optimized for the real main shocks and the minimum magnitude is sometimes adjusted for the real data, a uniform time window and magnitude range are used for the synthetics. As a result the C values for the synthetics produce a very different CDF than is found in either this study or the study by *Mignan et al.* [2006a].

[67] The problems associated with not acknowledging that earthquakes may be part of the AMR for multiple main shocks in the real catalog is also compounded by *Bowman et al.* [1998]. From their simulations, *Bowman et al.* [1998] find that the probability of obtaining a C value below 0.7 is 0.5 and then calculate the probability of finding 8 C values below 0.7 by assuming that the C values are independent. This makes the joint probability of obtaining 8 C values below 0.7 equal to 0.5^8 and makes their result for the real data appear to be significant at over the 99% confidence level. In fact, because the seismicity catalog is shared between all of the earthquakes, if one C value less than 0.7 is found then the chances are very good that other like values will be found as well. Thus the C values in the real data are not independent and their approach overestimates the statistical significance of the signal.

[68] The next two simulation methods we use include spatiotemporal clustering and the general spatial characteristics of the real data. The difference between the two simulations is that one uses a Gutenberg-Richter distribution to produce the magnitudes while the other uses an empirical distribution drawn from the real data. The simulation methods with clustering, as compared to those without clustering, produce distributions of C values that are even more similar to the one from the real data. Thus, when clustering is included, the K-S test rejects the AMR hypothesis. The effect of including clustering in the test is similar to the conclusions of *Michael* [1997] who studied the effect of seismicity clustering on a proposed electromagnetic precursor. This is because clustering, which exists in real data, can help artificial data fitting find unusual behavior. Therefore it is always important to include the effects of clustering in prediction tests. The synthetic catalogs of *Bowman et al.* [1998] and *Mignan et al.* [2006a] do not include spatiotemporal clustering, leading to poor simulation of C values in their synthetic tests. The fact that only our ETAS simulated catalogs matched the amount and distribution of AMR seen in the real catalog may also indicate, perhaps not too surprisingly, that the sudden rate increases occurring in aftershock and foreshock sequences of all sizes may accentuate apparent accelerations.

[69] We have found that spatiotemporal clustering in the form of aftershock sequences significantly increases the amount of apparent AMR that is found in a data set. One or several large aftershock sequences might lead to both a stronger apparent AMR signal and an increased chance of a large earthquake simply because larger earthquakes are more likely to occur during times of higher seismicity rates. This is because the higher the earthquake rate, the higher the probability of at least one large earthquake. Thus the existence of clustering makes AMR appear to be predictive. However, if the physical factor producing the apparent acceleration is aftershock clustering, forecasting of the probability of large earthquakes can be accomplished by existing applications of aftershock statistics via an ETAS [*Helmstetter et al.*, 2006] or STEP [*Gerstenberger et al.*, 2005] type model.

[70] We have focused on the AMR hypothesis as originally proposed by *Bowman et al.* [1998] rather than in one of many later studies that have proposed modifications in the hypothesis. One major change came when *Bowman and King* [2001] proposed using data selection regions based on Coloumb stress changes rather than circles around the impending main shock. By comparing the distribution of C values found for the circles and stress patterns in the real data, we show that this modification does not result in an improved AMR signal.

[71] This result is in contrast to those of *Mignan et al.* [2006a], who report lower values of C in positive prestress regions than in negative prestress regions. Their methodology was to determine the optimal circular area, and then to compare the positive and negative prestress regions within the optimal circle. However, the positive prestress region fills a larger portion of the circle than the negative prestress region (see their Figure 5), so the optimization of AMR in the circular area is weighted toward optimizing AMR in the positive prestress region, biasing the result. For 2 of the 9 main shocks, the negative prestress region inside the circle is so small that it contains <5 events. Further bias is introduced by assigning a value of $C = 1$ to the negative regions when less than 5 events are present, which guarantees that the positive prestress region will have a lower C value. Our tests do not contain this bias, since we optimize the positive prestress catalog and the whole catalog independently.

[72] There are many other proposed modifications and it is outside the scope of this study to examine each of them. Instead, the original authors should subject their proposals to rigorous statistical tests as we did for the paper of *Bowman et al.* [1998]. In addition to fully simulating the analysis process and using more realistic simulations of the seismicity, including clustering, these tests must include a large data set so the tests have sufficient statistical power. Case studies of individual events, or even several events, may be useful when developing a hypothesis but are inadequate for testing purposes.

9. Conclusions

[73] We have shown that apparent AMR in California and Nevada may result from a combination of data fitting and the spatiotemporal clustering of earthquakes. We compared real data with synthetic data sets containing no underlying AMR, including ETAS simulations with spatiotemporal clustering of earthquakes, and found the rate and strength of AMR in the real and ETAS catalogs to be indistinguishable. The high rate of observed AMR in all types of synthetic simulations demonstrates how easily apparent AMR can be found by optimizing the spatial and temporal windows. Proposed scaling relationships, which could help avoid artifacts of data fitting, have turned out to be both unstable and a statistical artifact of using a minimum magnitude that scales with the main shock magnitude.

[74] The difference between the amount of AMR found in random simulations and real data on one hand, and the similar amount found in the ETAS synthetics and real data

on the other, demonstrates the contribution of spatiotemporal earthquake clustering to apparent AMR. Observed AMR therefore does not imply any new earthquake behavior or physics, beyond the known occurrence of aftershocks and foreshocks. Given that AMR in retrospective tests appears to be an artifact of data fitting and earthquake-clustering, we speculate that in forward predictions AMR would have no more predictive power than clustering-based forecasts [e.g., *Gerstenberger et al.*, 2005; *Helmstetter et al.*, 2006; *Reasenberg and Jones*, 1989, 1994]. We prefer the clustering-based methods because they parameterize the earthquake clustering more directly.

[75] Our study focused on AMR as defined by *Bowman et al.* [1998], the foundation of most current AMR research. We also explored several more recent modifications, including spatial regions based on stress loading, removal of aftershocks before searching for AMR, and constraining the curvature parameter (m) to 0.3, and demonstrated that these modifications do not change the results. Other modifications to AMR are of course possible, and our study provides a model for testing any revised definition of AMR. In particular, if there is any true signal, it should be significantly stronger in real data than in ETAS simulations.

[76] Our results also have broader implications for the interpretation of other observed seismicity patterns. The spatiotemporal clustering of earthquakes makes it easy to find a desired pattern of seismicity rate changes, especially when there are adjustable parameters. For example, we found AMR in most random synthetic catalogs, and also found two conflicting patterns of acceleration and deceleration in many of the same real data sets. Similarly, other parameterizations of activation or quiescence, or more complex patterns, may also be easily found.

[77] Because a particular seismicity rate change pattern may be easy to find, a collection of retrospective case studies, even a large collection, does not prove the significance of an observed pattern. Statistical tests must be performed on a large data set and/or prospective testing must be undertaken. When testing the significance of observed seismicity patterns, the null hypothesis must include comparisons with synthetic catalogs with spatiotemporal clustering.

Appendix A: Catalogs With Synthetic Aftershocks

[78] Producing synthetic catalogs with spatiotemporal clustering resembling real seismicity is a complex task. We based our simulations on the ETAS model [e.g., *Ogata*, 1988] which provides temporal clustering based on the modified Omori relation. To produce the rate and spatial distribution of seismicity we need to seed the ETAS clusters with background earthquakes and then spatially distribute the events within the clusters.

[79] The times of the background earthquakes are chosen randomly, using a spatially varying background seismicity rate found from the real ANSS catalog using the technique of *Hainzl et al.* [2006]. The overall spatial character is less distinct in our synthetic ETAS catalogs than for the real data because of the 0.5°grid used to compute the spatially varying rate of background earthquakes (Figures 7a, 7g, and 7i). A smaller grid size would produce more spatially focused seismicity patterns but at the expense of less stable estimation of the background rates.

[80] Since it has been found that 60% of the earthquake catalog is made up of easily identifiable aftershocks [*Gardner and Knopoff*, 1974] the background seismicity rate should be equal to about 40% of the total seismicity rate. The ANSS earthquake catalog that we use has an average total seismicity rate of 67.2 M $\geq$ 4 earthquakes per year from 1950 to 2005, leading to an estimated background rate of 26.9 M $\geq$ 4 earthquakes/year. In comparison, the method of *Hainzl et al.* [2006] gives a total of 21.3 M $\geq$ 4 background earthquakes/year. The discrepancy may be because isolated areas with higher than average aftershock/background ratios contribute heavily to the total, and because the main shock rate estimated by the method of *Hainzl et al.* [2006] tends to be too low for catalogs with certain aftershock parameters. We correct for the difference by multiplying the background seismicity rates across the board by a factor of 1.26. Grid cells with no seismicity were given a small rate of main shocks such that in each simulation there is a 50% probability that one or more earthquakes will occur in the union of these grid cells.

[81] The ETAS simulations are implemented using the inverse transform method of *Felzer et al.* [2002]. In these simulations each earthquake, including each aftershock, may produce its own aftershocks. The total number of aftershocks produced per main shock varies as $\sim 10^{bM}$, where M is main shock magnitude and b is the b parameter in the Gutenberg-Richter magnitude frequency relationship [*Gutenberg and Richter*, 1944]. In the temporal domain the simulated aftershocks follow the modified Omori law [*Utsu*, 1961] given by $R(t) = K(t + c)^{-p}$, where t is time since the main shock, R is the aftershock rate, c and p are constants, and K is a value that varies with the magnitudes of the main shocks in question. Using the results of *Felzer et al.* [2002] we set $K = k10^{b(M-Maft)}$, where M is main shock magnitude, M_{aft} is the magnitude of the smallest aftershock counted, and k is an activity constant that is independent of magnitude.

[82] In *Felzer et al.* [2002] the smallest magnitude earthquake used in simulations, $M_{\min}$, was set to M 0. Here we increase $M_{\min}$ to 2.5. This is because we are doing a large simulation, over the entire states of California and Nevada for 55 years, and increasing $M_{\min}$ by a few units of magnitude saves on computational time substantially. The change in $M_{\min}$, however, also requires a corresponding change in the direct modified Omori law parameters. Note that the direct modified Omori parameters, which are the required input for the ETAS simulation, are the parameters that describe the rate of triggering of direct aftershocks only; they do not describe the combination of direct and secondary aftershocks that make up the full aftershock sequences observed in the field. It is very difficult to tease apart individual direct aftershock sequences from complete aftershock sequences observationally, making most direct parameters difficult to measure. An exception is the direct p parameter. It can be derived [*Sornette and Sornette*, 1999] and observed [*Felzer et al.*, 2003] that the p parameter for complete aftershock sequences changes with time, such that the average p value over a full sequence is close to 1.0 but the p value fit to data at long times is >1 and tends to

converge to the underlying direct p value. *Felzer et al.* [2003] found that California p values converge to about 1.34 at long times. Thus we set our direct p value to 1.34 and then grid search for the direct values of k and c. In the grid search the ETAS simulation is run with incremented parameter values, and the results are checked against the average ten and thirty day aftershock rates of $M \geq 4.7$ main shocks in California. The best fit parameters found for $M_{min} = 2.5$ are $k = 0.008$ days$^{(1-p)}$ and $c = 0.095$ days.

[83] The ETAS simulations of *Felzer et al.* [2002] are performed completely in the temporal domain. Here we add a spatial dimension by modeling each earthquake as a fault plane in 3D, with rupture dimensions taken from the relationships of *Wells and Coppersmith* [1994]. All faults are given a 90° dip, and 75% are randomly assigned a 303° strike (clockwise from north) and 25% a 213° strike, in accordance with our estimate of major fault trends in California. Aftershocks are placed in space such that their probability of being a distance, r, from the closest point on the fault plane of their main shock varies as $\sim r^{-1.3}$, in accordance with the empirical results of *Felzer and Brodsky* [2006]. Aftershock depth is limited to between 0 and 20 km. To avoid singularity at $r = 0$ aftershocks are not allowed closer than 1 meter from the main shock fault plane.

[84] For the magnitude distribution for the first set of simulations we follow *Felzer et al.* [2002], and assign the magnitude of each earthquake randomly from the Gutenberg-Richter distribution with a b value of 1.0. For the second set of simulations, we choose magnitudes randomly from the magnitudes listed in the ANSS catalog. Note that the total number of earthquakes in each ETAS simulation and in the ANSS catalog will not necessarily be the same because there is Poissonian randomness and positive feedback in the generation of ETAS aftershock sequences, leading to some unpredictability in total catalog size. As a result, some magnitudes will be randomly omitted or repeated.

[85] The ANSS catalog has some incompleteness at the smaller magnitudes and magnitude error, both of which bias the magnitude distribution upward [*Tinti and Mulargia*, 1985]. Thus, when we use ANSS magnitudes in the ETAS simulations, the higher values cause more aftershocks to be produced, and the simulated catalogs end up somewhat more active than the real catalog. Whereas the real catalog contains 42 $M \geq 6$ main shocks, for example, the ETAS simulations with ANSS-source magnitudes have a mean of 52, and a median of 49, $M \geq 6$ earthquakes per simulated catalog. When we perform the simulations using magnitudes from the pure G-R distribution, on the other hand, neither input nor output magnitudes are exaggerated and we end up with fewer than 42 main shocks; a median of 36 and a mean of 38 $M \geq 6$ earthquakes/simulated catalog. The standard deviation, however, is quite large, with the smallest ANSS and G-R simulated catalogs having only 19 and 25 $M \geq 6$ earthquakes, respectively, and the largest ones having 54 and 58. Thus our ETAS simulations span the number of earthquakes in the real catalog. To insure that the variability in the total number of earthquakes per simulated catalog itself will not affect our results we perform trials with purely random catalogs, altering the total earthquake rate from 0.25 to 4 times that seen in the real ANSS catalog, and measuring the value of C for random main shocks in each trial. We find no correlation between C values and the total number of earthquakes in the catalog over this range. In total for this test, we perform 20 ETAS simulations with each of the magnitude assignment methods described above. Hence our ETAS simulations are sufficiently accurate for the purposes of the tests done in this study.

[86] **Acknowledgments.** We thank David Bowman and Arnaud Mignan for several productive discussions. We are grateful to Sue Hough, Ken Hudnut, Roland Bürgmann, an anonymous reviewer, and the associate editor for their helpful reviews of the manuscript. We thank Ross Stein for suggesting we search for decelerating moment release. Several figures were prepared using the Generic Mapping Tools [*Wessel and Smith*, 1998]. All authors contributed equally to this article and the order was selected using a uniform random number generator.

References

Allen, C. R., A. Grantz, J. N. Brune, M. M. Clark, R. V. Sharp, T. G. Theodore, E. W. Wolfe, and M. Wyss (1968), The Borrego Mountain, California, earthquake of 9 April 1968: A preliminary report, *Bull. Seismol. Soc. Am.*, *58*, 1183–1186.

Benioff, H. (1951), Earthquakes and rock creep. part I: Creep characteristics of rocks and the origin of aftershocks, *Bull. Seismol. Soc. Am.*, *41*, 31–62.

Bowman, D. D., and G. C. P. King (2001), Accelerating seismicity and stress accumulation before large earthquakes, *Geophys. Res. Lett.*, *28*(21), 4039–4042.

Bowman, D. D., G. Ouillon, C. G. Sammis, A. Sornette, and D. Sornette (1998), An observational test of the critical earthquake concept, *J. Geophys. Res.*, *103*(10), 24,359–24,372.

Bufe, C. G., and D. J. Varnes (1993), Predictive modeling of the seismic cycle of the greater San Francisco Bay region, *J. Geophys. Res.*, *98*(B6), 9871–9883.

Caskey, S. J., S. G. Wesnousky, P. Zhang, and D. B. Slemmons (1996), Surface faulting of the 1954 Fairview Peak (Ms 7.2) and Dixie Valley (M (sub S) 6.8) earthquakes, central Nevada, *Bull. Seismol. Soc. Am.*, *86*, 761–787.

Doser, D. I. (1986), Earthquake processes in the Rainbow Mountain-Fairview Peak-Dixie Valley, Nevada, region 1954–1959, *J. Geophys. Res.*, *91*(B12), 12,572–12,586.

Ebel, J. E., and D. V. Helmberger (1982), P-wave complexity and fault asperities: The Borrego Mountain, California, earthquake of 1968, *Bull. Seismol. Soc. Am.*, *72*, 413–437.

Felzer, K. R., and E. E. Brodsky (2006), Decay of aftershock density with distance indicates triggering by dynamic stress, *Nature*, *441*, 735–738.

Felzer, K. R., T. W. Becker, R. E. Abercrombie, G. Ekstrom, and J. R. Rice (2002), Triggering of the 1999 Mw 7.1 Hector Mine earthquake by aftershocks of the 1992 Mw 7.3 Landers earthquake, *J. Geophys. Res.*, *107*(B9), 2190, doi:10.1029/2001JB000911.

Felzer, K. R., R. E. Abercrombie, and G. Ekstrom (2003), Secondary aftershocks and their importance for aftershock prediction, *Bull. Seismol. Soc. Am.*, *93*, 1433–1448.

Gardner, J. K., and L. Knopoff (1974), Is the sequence of earthquakes in southern California, with aftershocks removed, Poissonian?, *Bull. Seismol. Soc. Am.*, *64*, 1363–1367.

Gerstenberger, M., S. Wiemer, L. Jones, and P. Reasenberg (2005), Real-time forecasts of tomorrow's earthquakes in California, *Nature*, *435*, 328–331.

Gutenberg, B., and C. F. Richter (1944), Frequency of earthquakes in California, *Bull. Seismol. Soc. Am.*, *34*, 185–188.

Hainzl, S., F. Scherbaum, and C. Beauval (2006), Estimating background activity based on interevent-time distribution, *Bull. Seismol. Soc. Am.*, *96*, 313–320.

Heaton, T., and D. V. Helmberger (1979), Generalized ray models of the San Fernando earthquake, *Bull. Seismol. Soc. Am.*, *69*, 1311–1341.

Helmstetter, A., Y. Y. Kagan, and D. D. Jackson (2006), Comparison of short-term and time-dependent earthquake forecast models for southern California, *Bull. Seismol. Soc. Am.*, *96*, 90–106.

Ji, C., D. J. Wald, and D. V. Helmberger (2002), Source description of the 1999 Hector Mine, California, earthquake. part II: Complexity of slip history, *Bull. Seismol. Soc. Am.*, *92*, 1208–1226.

Ji, C., K. L. Larson, Y. Tan, K. W. Hudnut, and K. Choi (2004), Slip history of 2003 San Simeon earthquake constrained by combining 1-Hz GPS, strong motion, and teleseismic data, *Geophys. Res. Lett.*, *31*, L17608, doi:10.1029/2004GL020448.

Jiang, C., and Z. Wu (2005), Test of preshock accelerating moment release (AMR) in the case of the 26 December 2004 Mw9.0 Indonesia earthquake, *Bull. Seismol. Soc. Am.*, *95*, 2016–2025.

Kanamori, H. (1981), The nature of seismicity patterns before large earthquakes, in *Earthquake Prediction An International Review*, edited by D. W. Simpson and P. G. Richards, pp. 1–19, AGU, Washington, D. C.

Kanamori, H., and D. L. Anderson (1975), Theoretical basis of some empirical relations in seismology, *Bull. Seismol. Soc. Am.*, *65*, 1073–1095.

Keilis-Borok, V. I., and V. G. Kossobokov (1990), Times of increased probability of strong earthquakes (M $\geq$ 7.5) diagnosed by algorithm M8 in Japan and adjacent territories, *J. Geophys. Res.*, *95*(B8), 12,413–12,422.

King, G. C. P., and D. D. Bowman (2003), The evolution of regional seismicity between large earthquakes, *J. Geophys. Res.*, *108*(B2), 2096, doi:10.1029/2001JB000783.

Matthews, M. V., and P. A. Reasenberg (1988), Statistical methods for investigating quiescence and other temporal seismicity patterns, *Pure Appl. Geophys.*, *126*(2–4), 357–372.

Michael, A. J. (1997), Testing prediction methods; earthquake clustering versus the Poisson model, *Geophys. Res. Lett.*, *24*(15), 1891–1894.

Mignan, A., D. Bowman, and G. King (2006a), An observational test of the origin of accelerating moment release before large earthquakes, *J. Geophys. Res.*, *111*, B11304, doi:10.1029/2006JB004374.

Mignan, A., G. King, D. Bowman, R. Lacassin, and R. Dmowska (2006b), Seismic activity in the Sumatra-Java region prior to the December 26, 2004 (Mw = 9.0–9.3) and March 28, 2005 (Mw = 8.7) earthquakes, *Earth Planet. Sci. Lett.*, *244*(3–4), 639–654.

Ogata, Y. (1988), Statistical models of point occurrences and residual analysis for point processes, *J. Am. Stat. Assoc.*, *83*, 9–27.

Okada, Y. (1992), Internal deformation due to shear and tensile faults in a half-space, *Bull. Seismol. Soc. Am.*, *82*, 1018–1040.

Reasenberg, P. A., and M. V. Matthews (1988), Precursory seismic quiescence: A preliminary assessment of the hypothesis, *Pure Appl. Geophys.*, *126*(2–4), 373–406.

Reasenberg, P. A., and L. M. Jones (1989), Earthquake hazard after a mainshock in California, *Science*, *243*(4895), 1173–1176.

Reasenberg, P., and L. Jones (1994), Earthquake aftershocks: Update, *Science*, *265*, 1251–1252.

Reyners, M. (1981), Long- and intermediate-term seismic precursors to earthquakes; state of the art, in *Earthquake Prediction; An International Review*, *Maurice Ewing Ser.*, vol. 4, edited by D. W. Simpson and P. G. Richards, pp. 333–347, AGU, Washington, D.C.

Savage, J. C., and R. O. Burford (1973), Geodetic determination of relative plate motion in central California, *J. Geophys. Res.*, *78*(5), 832–845.

Sornette, A., and D. Sornette (1999), Renormalization of earthquake aftershocks, *Geophys. Res. Lett.*, *26*(13), 1981–1984.

Tiampo, K. F., J. B. Rundle, W. Klein, and J. R. Holliday (2006), Forecasting rupture dimension using the pattern informatics technique, *Tectonophysics*, *424*(3–4), 367–376.

Tinti, S., and F. Mulargia (1985), Effects of magnitude uncertainties on estimating parameters in the Gutenberg-Richter frequency-magnitude law, *Bull. Seismol. Soc. Am.*, *75*, 1681–1697.

Toppozada, T. R., and D. M. Branum (2002), California earthquakes of M>5: Their history and areas damaged, in *International Handbook of Earthquake and Engineering Seismology (Part A)*, edited by W. H. K. Lee et al., pp. 793–796, Academic Press, New York.

Uhrhammer, R. A., S. J. Lober, and B. Romanowicz (1996), Determination of local magnitude using BDSN broadband records, *Bull. Seismol. Soc. Am.*, *86*, 1314–1330.

Utsu, T. (1961), A statistical study on the occurrence of aftershocks, *Geophys. Mag.*, *30*, 521–605.

Wald, D. J., and T. Heaton (1994), Spatial and temporal distribution of slip for the 1992 Landers, California, earthquake, *Bull. Seismol. Soc. Am.*, *84*, 668–691.

Wald, D. J., D. V. Helmberger, and S. Hartzel (1990), Rupture process of the 1987 Superstition Hills earthquake from the inversion of strong-motion data, *Bull. Seismol. Soc. Am.*, *81*, 1540–1572.

Wald, D. J., D. V. Helmberger, T. H. Heaton, T. C. Hanks, and H. Krawinkler (1991), Rupture model of the 1989 Loma Prieta earthquake from the inversion of strong-motion and broadband teleseismic data, *Bull. Seismol. Soc. Am.*, *81*(5), 1540–1572.

Wald, D. J., T. Heaton, and K. W. Hudnut (1996), The slip history of the 1994 Northridge, California, earthquake determined from strong-motion, teleseismic, GPS, and leveling data, *Bull. Seismol. Soc. Am.*, *86*, S49–S70.

Wells, D. L., and K. J. Coppersmith (1994), New empirical relationships among magnitude, rupture length, rupture width, rupture area, and surface displacement, *Bull. Seismol. Soc. Am.*, *84*(4), 974–1002.

Wessel, P., and W. H. F. Smith (1998), New, improved version of the Generic Mapping Tools released, *Eos Trans. AGU*, *79*(47), 579.

K. R. Felzer, U.S. Geological Survey, 525 South Wilson Avenue, Pasadena, CA 91106, USA. (kfelzer@gps.caltech.edu)

J. L. Hardebeck and A. J. Michael, U.S. Geological Survey, MS 977, 345 Middlefield Road, Menlo Park, CA 94025, USA. (jhardebeck@usgs.gov; michael@usgs.gov)